W-Band Micromachined Circuit Combining Networks

Katherine J. Herrick and Linda P. B. Katehi

***Abstract*—In circuit-combining networks, low-loss interconnecting transmission lines are pivotal in reducing excess loss. Micromachined finite ground coplanar waveguides are used in this study as low-loss interconnects showing significant improvements in line loss while maintaining 50-Ω characteristic impedance. Wilkinson power dividers, reactive tee junctions, and right-angle bends are combined with micromachined interconnects in 1 : 2, 1 : 4, and 1 : 8 power-dividing networks and show measured loss reduction of 0.3–1.0 dB depending on circuit type and size from 85 to 95 GHz.**

***Index Terms*—Micromachining, microwave circuits, packaging.**

I. Introduction

With the advancements of high-density and multilayer circuit applications comes the continued emphasis on low-loss low-cost transmission lines. In power-dividing networks, in which power is split from 1 to 4 or more signal paths, the transmission-line characteristics become significant since longer lines are typically required. One power-dividing application is the excitation of radiating elements, such as patch antennas of $\lambda_g/2$ in size and center-to-center spacing of $\lambda_o/2$. In Fig. 1, both 1 : 4 and 1 : 8 networks are displayed in which an individual signal path from the input to one radiating element is illustrated as $Ax + By$. Although the y-dimension requirements are less stringent, the x-dimension requirements are dictated by the size of the radiation elements and their spacing. The 1 : 8 layout requires twice as much circuit length from the input to one radiating element as compared to the 1 : 4 layout. Thus, interconnecting line loss may become the dominant loss mechanism despite the presence of low-loss power-splitting elements such as Wilkinsons and reactive tee junctions.

As shown previously in the literature, the micromachined finite ground coplanar (MFGC) waveguide has demonstrated significantly lower loss than the conventional coplanar waveguide for frequencies up to 110 GHz [1]–[3]. By simply micromachining the silicon from the aperture regions of the line, loss improvements can be made without sacrificing the structural integrity, double-sided processing, and modifying the aspect ratio. Arguably, the localization of the fields also makes this line a better multilayer candidate than microstrip. However, in addition to decreasing the attenuation of the line, micromachining the aperture regions decreases the effective dielectric constant, thereby increasing the characteristic impedance. Thus, geometry modifications must be made to match a particular impedance to a micromachined line.

This study focuses on the application of MFGC lines in circuit-combining networks [4], [5]. Rather than redesign components such as Wilkinsons and reactive tee junctions, the intent here is to develop MFGC feed lines that maintain a base characteristic impedance, as well as provide significantly lower ohmic loss. In this paper, the modeling and measurement of 50-Ω lines is first presented, and is followed by theoretical and experimental verification of the component performance. The interconnect lines and components are then integrated into circuit-combining networks to demonstrate loss improvements obtained through micromachining. Both theoretical and experimental results show substantial loss reduction when the lines are micromachined in one to two (1 : 2), one to four (1 : 4), and one to eight (1 : 8) power-dividing networks.

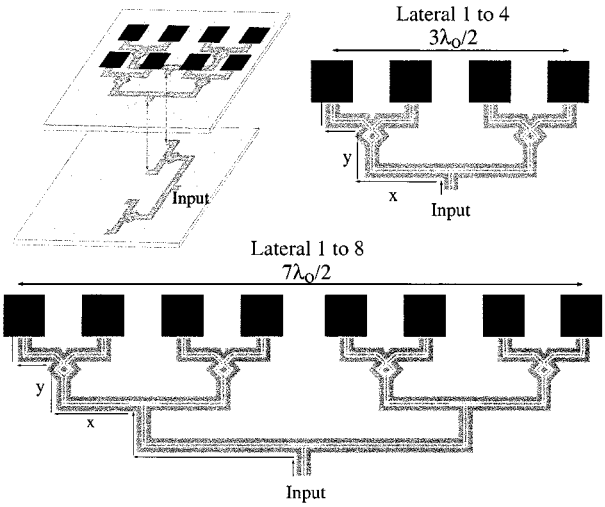

Fig. 1. 1 : 4 and 1 : 8 networks with respective signal line lengths. Distance from input to radiating element for 1 : 4 is $1.5x + By$ and for 1 : 8 is $3.0x + By$.

II. Components

A. Design

The components used for the circuit-combining networks are Wilkinson power dividers, reactive tee junctions, and right-angle bends. These components have been discussed in the literature [4], [5]. The feed-line dimensions are 40-μm center conductor, 24-μm apertures, and 106-μm ground planes. All of the 50-Ω designs incorporate compensations for the capacitive loading effect of air bridges on the transmission line. An examination of compensations for single air bridges has been presented in the literature [6], [7], where an air bridge is modeled as a shunt capacitance and its equivalent low impedance is compensated with high-impedance sections.

B. Measurements

S-parameters of the combining networks are measured on an HP 8510C Network Analyzer[1] using 150-μm pitch Picoprobes[2] and a thru-reflect line (TRL) calibration method to deembed the probe-to-wafer transition. This method of deembedding establishes reference planes at the input and output ports of the circuits under test[3] [8].

Measurement of the individual components requires right-angle orientation of the measurement probes. As the W-band setup requires the probes to be aligned and facing each other, a right-angle bend is added to each of the components for measurement purposes. Thus, the three

Manuscript received October 18, 2000; revised May 16, 2001. This work was supported by the Office of Naval Research under Contract N00014-95-1-0546, and by the Defense Advanced Research Projects Agency/Electronics Technology Office under Contract N66001-96-C-8635.

K. J. Herrick was with the Radiation Laboratory, Department of Electrical Engineering and Computer Science, The University of Michigan at Ann Arbor, Ann Arbor, MI 49109-2122 USA. She is now with Raytheon RF Components, Andover, MA 01810 USA (e-mail: kherrick@raytheon.com).

L. P. B. Katehi was with the Radiation Laboratory, Department of Electrical Engineering and Computer Science, The University of Michigan at Ann Arbor, Ann Arbor, MI 49109-2122 USA. She is now with the Office of the Dean of Engineering, Purdue University, West Lafayette, IN 47907-1280 USA (e-mail: katehi@purdue.edu).

Publisher Item Identifier S 0018-9480(02)05216-X.

[1]Hewlett-Packard, Santa Clara, CA.

[2]GGB Industries, Naples, FL.

[3]R. B. Marks and D. F. Williams, *Multical v1.00*, Nat. Inst. Stand. Technol. (NIST), Boulder, CO, 1995.

TABLE I
ESTIMATED COMPONENT INSERTION-LOSS VALUES AT 90 GHz AS TAKEN FROM MEASUREMENT WITH MEASUREMENT ERROR DENOTED

Component	Component Loss
50 Ω Wilkinson	0.40 ± 0.03 dB
50 Ω reactive tee	0.24 ± 0.05 dB
50 Ω right angle bend	0.11 ± 0.03 dB

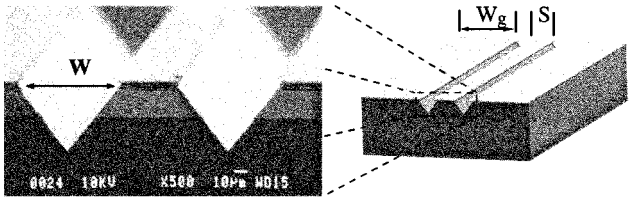

Fig. 2. MFGC geometry.

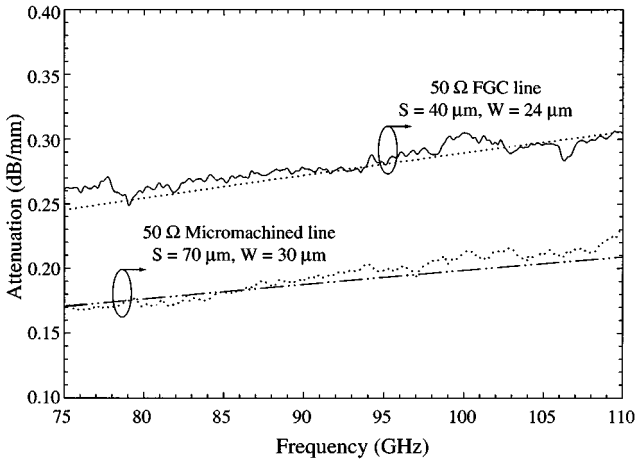

Fig. 3. Measured attenuation for FGC line and micromachined FGC line of the same characteristic impedance as compared to modeled.

TABLE II
ELECTRO-STATIC CHARACTERISTICS OF MICROMACHINED AND UNMICROMACHINED (CONVENTIONAL) LINES

Design	S/W (μm)	C_{sub} (pF/m)	C_{air} (pF/m)	ϵ_{eff}	Z_o (Ω)
50 Ω FGC	40/24	170	27	6.2	54
50 Ω MFGC	70/30	140	29	4.7	52

TABLE III
MEASURED AND MODELED ATTENUATION VALUES FROM 85 TO 95 GHz

Design	S/W (μm)	α (dB/mm) Measured	α (dB/mm) Modeled
50 Ω FGC	40/24	0.260-0.280	0.255-0.280
50 Ω MFGC	70/30	0.180-0.200	0.180-0.195

circuits measured for component loss extraction are: 1) Wilkinson and bend; 2) reactive tee and bend; and 3) double bend. The measured values at 90 GHz are averaged and assigned a margin of error based on the ripple in the measurement. The attenuation of the interconnecting lines is deembedded from the measurement and the remaining insertion loss represents that of the tested component. Table I shows the measured loss for each component. These loss values will be used with the measured interconnect line loss to predict and compare total loss in various circuit-combining networks to be presented.

III. INTERCONNECTS

A. Design

Design of the MFGC waveguide shown in Fig. 2 begins with electrostatic simulations of the cross section of the line.[4] Note these electrostatic simulations are based on a two-dimensional (2-D) finite-element method. This technique allows for accurate modeling of the line architecture, including 5000 Å of SiO_2 underneath each of the three conductors. In addition, no lateral undercut of silicon under the conductive regions is assumed in the model [1], [2]. From the calculated line shunt capacitance, the effective dielectric constant and characteristic impedance are obtained, as shown in Table II, for micromachined and conventional 50-Ω transmission lines. The center conductor width is increased by 30 μm to maintain a 50-Ω line when the 30-μm apertures are etched. Although $S + 2W$ is wider for the micromachined case, radiation loss will not increase if $S + 2W \leq \lambda_g/10$ [9]. In this case, $\lambda_g/10 = 136$ μm at 90 GHz and the radiation condition is met.

The series resistance and inductance per unit length for the two lines as a function of frequency are obtained using a 2-D surface ribbon method, which takes into account the cross section of the three 1-μm conductors alone [10], [11]. The conductivity used for all lines is 3.7×10^7 S/m. The 50-Ω micromachined line yields the lowest series resistance and inductance values due to its 70-μm-wide center conductor. For example, at 95 GHz, the series resistance and inductance per unit length for the micromachined and conventional FGC 50-Ω lines are 2200 Ω/m, 3.9×10^{-7} H/m and 3300 Ω/m, 4.2×10^{-7} H/m, respectively. Fig. 3 shows the modeled attenuation from (1) versus frequency for each line. At 90 GHz, attenuation values of 0.27 and 0.19 dB/mm are predicted for the conventional and micromachined lines, respectively. Thus, the micromachined version yields 0.8-dB/cm loss improvement

$$\alpha = \mathrm{Re}\sqrt{(R + jwL)(jwC_{\mathrm{sub}})}. \tag{1}$$

[4]*Maxwell 2-D*, ver. 1.9.04, Ansoft Corporation, Pittsburgh, PA, 1997.

B. Measurements

A separate calibration set is used for each of the geometries tested (50-Ω finite ground coplanar (FGC), 50-Ω MFGC), and the measured attenuation based on each calibration is shown in Fig. 3. These measured results are superimposed with the modeled results showing close match of both lines, which is obtained by using 2-D methods that allow for modeling of the exact architecture including finite thickness of all conductors and dielectrics. The results have been tabulated showing attenuation values for both measured and modeled lines in decibels/millimeter at 90 GHz (see Table III). The attenuation of the conventional 50-Ω line is 0.27 dB/mm at 90 GHz, while the micromachined version reduces the loss to 0.19 dB/mm at 90 GHz.

IV. FABRICATION

The circuits are printed on 400-μm-thick high-resistivity double-side polished silicon wafers with 6600-Å SiO_2 on both sides. The five main fabrication steps are: 1) thin-film resistor deposition; 2) circuit metallization; 3) aperture definition; 4) air-bridge formation; and 5) anisotropic wet etching of the apertures. Nichrome (NiCr) is used for the thin-film resistors, as it is not etched in potassium hydroxide (KOH), the anisotropic etchant used to create the micromachined grooves.

For the thin-film resistors, 400 Å of NiCr is deposited using a liftoff process. This thickness results in a sheet resistance of 42 Ω/square

Fig. 4. Photographs of fabricated 1 : 2 networks including one Wilkinson, one right-angle bend, and 2.1-mm interconnect length for each of two signal paths.

based on a four-point probe measurement. A liftoff process is also used for the circuit metallization of Cr/Au (500/9500 Å), and silicon dioxide is patterned in the aperture regions and etched in buffered hydrofluoric acid (BHF) for 6.6 min (1000-Å/min etch rate). Flood evaporation of a seed layer [Cr/Au/Cr (500/1000/500 Å)] initiates air-bridge formation. After patterning, the bridges are electroplated in a cyanide-based solution to approximately 3 μm, and removal of the seed layers completes the air-bridge formation. The final step is to anisotropically etch the oxide-patterned apertures in potassium hydroxide (KOH) at an etch rate of 30 Å/h. Note that KOH yields a minimal amount of lateral undercut, although substantial lateral undercut may be achieved using other anisotropic wet etchants such as ethylene diamene pyrocatechol (EDP) and tetramethyl ammonium hydroxide (TMAH) [1], [2], [12]. As stated previously, lateral undercut was not utilized in this particular research effort.

V. 50-Ω Circuit-Combining Networks

A. Design

Three circuit-combining networks will now be presented with 1 : 2, 1 : 4, and 1 : 8 power division. In addition to differences in the number of components required for the desired signal division, interconnecting line lengths differ as well. In this study, the interconnecting line lengths for the 1 : 2, 1 : 4, and 1 : 8 50-Ω networks are 2.1, 5.7, and 6.8 mm, respectively.

Micromachined and conventional networks are shown in Figs. 4–6. In Fig. 4, the electrical signal for each of the two 1 : 2 networks travels through a Wilkinson, a section of line, and a right-angle bend, resulting in 3 dB of nominal loss. Shown in Fig. 5 are fabricated 1 : 4 networks in which the input signal travels through 5.7 mm of interconnects, a reactive tee junction, two right-angle bends, and one Wilkinson power divider, yielding 6-dB nominal loss. Lastly, Fig. 6 shows photographs of two 1 : 8 networks consisting of one reactive tee, two Wilkinsons, and three right-angle bends for each of eight signal paths. The total interconnecting length is approximately 6.8 mm for each signal path, which is physically required for this network, and has 9-dB nominal insertion loss.

B. Measurements

Table IV summarizes the insertion loss results for the 1 : 2 (2.1-mm interconnect), 1 : 4 (5.7-mm interconnect), and 1 : 8 (6.8-mm interconnect) circuit-combining networks presented at 90 GHz. As a measure of consistency, the tabular loss summary includes the estimated loss taken as the sum of the measured component losses (Table I) and interconnect line attenuation (Table III) at 90 GHz. Close comparison of the measured and estimated network insertion loss will not only validate the measured results, but show consistency in the measurements. The IE3D/Libra modeled loss is given as a third benchmark.

For example, the conventional 1 : 2 design includes 2.1 mm of interconnect line resulting in an estimated loss of approximately 0.6 dB. The measured component loss, as taken from Table I, for the Wilkinson and the right-angle bend is approximately 0.5 dB. Since the estimated loss is the sum of the measured interconnecting line loss and the measured component loss, the estimated loss for the conventional 1 : 2 network is approximately 1.1 dB. Estimated loss for each network shown is calculated in the same manner and given in Table IV.

The measured and modeled loss data in Table IV for 1 : 2 networks were taken from Fig. 7, in which the measured and modeled excess insertion loss (S_{21}) is plotted versus frequency for these circuits with 2.1-mm total interconnect length. The measured 50-Ω conventional circuit yields excess insertion loss of 1.2 dB at 90 GHz, while the micromachined version reduces the loss to 0.9 dB, which represents a 30% reduction in loss and a 10% increase in combining efficiency. Modeled results of the entire circuit, including the 2.1 mm of interconnects, show the micromachined circuit with excess insertion loss values of 0.75 dB; 0.15 dB less than the 50-Ω measured results. The modeled insertion loss for the 50-Ω conventional circuit yields 0.9-dB excess insertion loss at 90 GHz. Thus, the model predicts a 0.15-dB loss reduction while measured results yield 0.3-dB improvements.

Examining the three benchmarks for the 1 : 2 networks, the estimated loss matches the measured loss ± 0.1 dB, while the modeled loss is lower than both estimated and measured losses by 0.15–0.3 dB. These results match favorably and show modeled loss to be conservative as predicted. All three loss benchmarks indicate insertion loss improvement of 0.15–0.3 dB with micromachining.

The model (not shown) for the 1 : 4 networks with 5.7 mm of interconnect line predicts insertion loss values of 2.2 dB above the nominal for the conventional 50-Ω designs at 90 GHz, while the micromachined version improves loss to 2.0 dB. Measured loss data for the 1 : 4 networks is taken from Fig. 8 displaying similar improvements with 2.7-dB excess loss reduced to 2.1 dB with the micromachined circuit design at 90 GHz. This modeled and measured data is summarized in Table IV with the estimated loss. The conventional estimated loss is approximately 2.4, which is 0.3 dB less than the total loss measured and 0.2 dB more than the model predicted loss. For the micromachined case, the estimated loss is 1.94 dB and the measured loss is 2.1 dB, matching that of the model well. Thus, the estimated and measured benchmarks indicate insertion loss improvement of 0.5–0.6 dB with micromachining for this particular 1 : 4 design.

Fig. 9 demonstrates the potential in combining efficiency when interconnect lengths are extended up to 7 mm in a 1 : 4 combining network. A schematic of the combining circuit is embedded in this figure. Modeled excess loss and combining efficiency, beyond the nominal 6 dB, are plotted versus interconnect length for combining networks of conventional and micromachined lines. The overall effect of micromachined circuits, as circuit lengths are increased, is a further reduction of loss and improvement in combining efficiency. For example, a network of 4 mm in interconnect length provides 2.0 dB of excess loss for the 50-Ω conventional 1 : 4 circuit according to the modeled data. When micromachining is applied, excess losses are reduced to 1.7 dB. For a network of 5.0 mm, additional loss improvements are obtained using micromachining. In this case, loss is reduced from 2.3 to 1.9 dB, with a 6% improvement in efficiency. This difference of 0.4 dB can be quite substantial in a system with a goal, for example, of only 2-dB total loss and becomes even more beneficial when several combining networks are used for multilayer applications or longer combining networks.

Also shown in Fig. 9 are the measured values for the 50-Ω networks, presented as triangular data points. Data points at 90 GHz from Fig. 8 are plotted at 5.7 mm on Fig. 9 as well as the most compact 1 : 4 network measured with 1.1 mm of interconnect length.

In measuring a 1 : 4 network, in which three of the four output ports are terminated with matched thin-film resistors, it is important to establish power balance in each of the four signal paths. Ideally, one network would be fabricated and probes would be placed on the input port and on each of the four output ports. Since this measurement setup is unavailable, four identical 1 : 4 networks are fabricated and each of the four output ports are measured separately. All four measurements

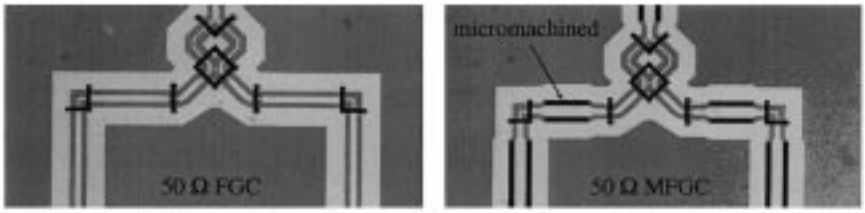

Fig. 5. Photographs of fabricated 1 : 4 networks including one Wilkinson, one reactive tee junction, two right-angle bends, and 5.7-mm interconnect length for each of four signal paths.

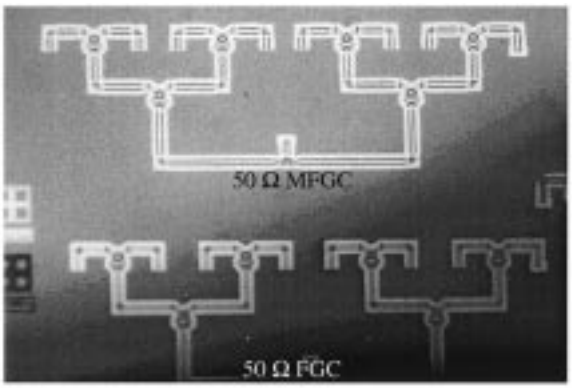

Fig. 6. Photographs of fabricated 1 : 8 networks including two Wilkinsons, one reactive tee junction, three right-angle bends, and 6.8-mm interconnect length for each of eight signal paths.

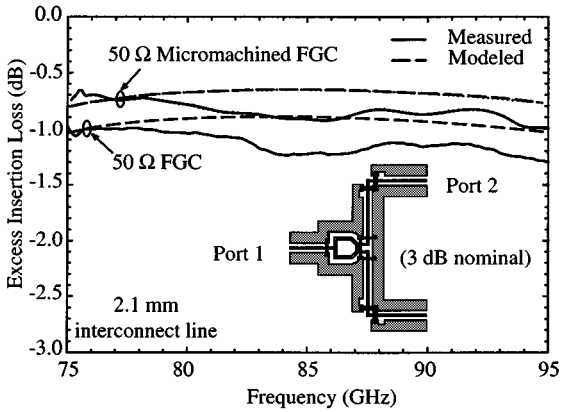

Fig. 7. Measured and modeled excess insertion loss (above 3 dB nominal) of four Wilkinson plus bend circuits with 2.1-mm interconnect length.

TABLE IV
ESTIMATED EXCESS LOSS FOR 1 : 2, 1 : 4, AND 1 : 8 CIRCUIT NETWORKS AS COMPARED WITH MEASURED AND SIMULATED RESULTS AT 90 GHz. MEASUREMENT ERROR IS ±0.1 dB

Design 1:2	Est. loss (dB)	Meas. loss (dB)	Mod. loss (dB)
50 Ω FGC	1.1	1.2	0.9
50 Ω MFGC	0.9	0.9	0.75
Δ 50	0.2	0.3	0.15
Design 1:4	**Est loss (dB)**	**Meas loss (dB)**	**IE3D loss (dB)**
50 Ω FGC	2.4	2.7	2.2
50 Ω MFGC	1.9	2.1	2.0
Δ 50	0.5	0.6	0.2
Design 1:8	**Est loss (dB)**	**Meas loss (dB)**	**IE3D loss (dB)**
50 Ω FGC	3.2	3.1	3.1
50 Ω MFGC	2.6	2.1	2.7
Δ 50	0.6	1.0	0.4

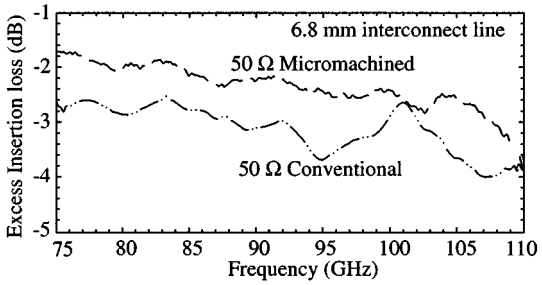

Fig. 8. Measured excess insertion loss for 1 : 4 combining network with 5.6-mm interconnect length.

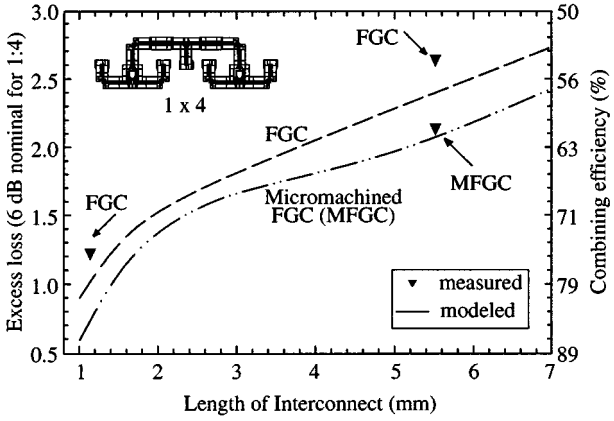

Fig. 9. Excess loss and combining efficiency versus interconnect length at 90 GHz for 1 : 4 networks.

match closely, with insertion loss of 1.2 dB at 90 GHz±0.1 dB. The expected loss for this network at the same frequency is 1.2, which is the sum of the expected 0.84-dB component loss and the 0.33-dB line loss. The measured phase for the four networks was nearly identical as well.

Lastly, Table IV summarizes the excess insertion losses of the two 1 : 8 networks at 90 GHz with the following three benchmarks:

1) estimated loss;
2) actual measured loss;
3) modeled loss.

The conventional 50-Ω design includes 6.7 mm of interconnect line resulting with an estimated loss of approximately 1.9 dB for the interconnects alone. The measured component loss, as taken from Table I, is approximately 1.34 dB, and summing these losses yields 3.2 dB of estimated loss for the conventional 1 : 8 network. For the micromachined case, the estimated loss is 2.6 dB, a 0.6-dB improvement is, therefore, predicted.

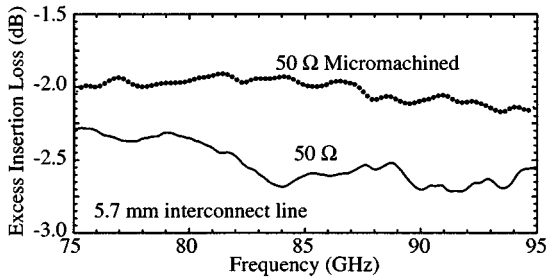

Fig. 10. Measured excess insertion loss for $1:8$ combining networks with 6.8-mm interconnect length.

Measured S-parameter results for the conventional 50-Ω $1:8$ case yield return losses below -17 dB from 75 to 110 GHz, and insertion loss values of approximately 3 dB above the 9 dB nominal at 90 GHz. The insertion loss is plotted with that of the micromachined design in Fig. 10. At 90 GHz, the micromachined circuit yields insertion losses close to 2.0 dB above nominal, a 1-dB improvement. Overall, the three loss benchmarks for the $1:8$ networks indicate insertion loss improvement of 0.4–1.0 dB with micromachining.

VI. Conclusion

While maintaining a particular characteristic impedance, MFGC waveguides provide lower loss than the conventional alternative. When implemented into circuit-combining networks in which half or more power is lost nominally, MFGC interconnects between components significantly reduce the excess loss. This loss improvement becomes more prominent with larger or multilayer networks.

References

[1] K. J. Herrick, T. A. Schwarz, and L. P. B. Katehi, "W-band micromachined finite ground coplanar (FGC) line circuit elements," in *IEEE MTT-S Int. Microwave Symp. Dig.*, vol. 1, Denver, CO, June 1997, pp. 269–272.

[2] ——, "Si-micromachined coplanar waveguides for use in high-frequency circuits," *IEEE Trans. Microwave Theory Tech.*, vol. 46, no. 6, pp. 762–768, June 1998.

[3] K. J. Herrick, J. G. Yook, and L. P. B. Katehi, "Microtechnology in the development of three-dimensional circuits," *IEEE Trans. Microwave Theory Tech.*, vol. 46, pp. 1832–1844, Nov. 1998.

[4] T. M. Weller, R. M. Henderson, K. J. Herrick, S. V. Robertson, R. T. Kihm, and L. P. B. Katehi, "Three-dimensional high-frequency distribution networks—Part 1: Optimization of CPW discontinuities," *IEEE Trans. Microwave Theory Tech.*, vol. 48, pp. 1635–1642, Oct. 2000.

[5] R. M. Henderson, K. J. Herrick, T. M. Weller, S. V. Robertson, R. T. Kihm, and L. P. B. Katehi, "Three-dimensional high-frequency distribution networks part 2: Packaging and integration," *IEEE Trans. Microwave Theory Tech.*, vol. 48, pp. 1643–1651, Oct. 2000.

[6] T. M. Weller, R. M. Henderson, and L. P. B. Katehi, "Optimization of MM-wave distribution networks using silicon-based CPW," in *IEEE MTT-S Int. Microwave Symp. Dig.*, June 1998, pp. 537–540.

[7] E. Rius, J. P. Coupez, S. Toutain, C. Person, and P. Legaud, "Theoretical and experimental study of various types of compensated dielectric bridges for millimeter-wave coplanar applications," *IEEE Trans. Microwave Theory Tech.*, vol. 48, pp. 152–156, Jan. 2000.

[8] R. B. Marks, "A multiline method of network analyzer calibration," *IEEE Trans. Microwave Theory Tech.*, vol. 39, pp. 1205–1215, July 1991.

[9] D. B. Rutledge, D. P. Neikirk, and D. P. Kasilingham, "Integrated-circuit antennas," in *Millimeter Components and Techniques, Part II*, K. J. Button, Ed. New York: Academic, 1983, vol. 10, Infrared and Millimeter Waves, ch. 1, pp. 1–90.

[10] Surface impedance method for interconnect analysis, S. Kim, E. Tuncer, B.-T. Lee, and D. P. Neikirk. (1997). [Online]. Available: http://wee-wave.mer.utexas.edu/MedHome.html

[11] E. Tuncer, B.-T. Lee, and D. P. Neikirk, "Interconnect series impedance determination using a surface ribbon method," in *3rd Topical Elect. Performance Electron. Packag. Meeting*, Nov. 1994, pp. 250–252.

[12] M. Madou, *Fundamentals of Microfabrication*. Boca Raton, FL: CRC Press, 1997.